

High resolution AMI Large Array imaging of spinning dust sources: spatially correlated $8\,\mu\text{m}$ emission and evidence of a stellar wind in L675^{*}

AMI Consortium: Anna M. M. Scaife¹†, David A. Green¹, Guy G. Pooley¹, Matthew L. Davies¹, Thomas M. O. Franzen¹, Keith J. B. Grainge², Michael P. Hobson¹, Natasha Hurley-Walker¹, Anthony N. Lasenby², Malak Olamaie¹, John S. Richer², Carmen Rodríguez-Gonzálvez¹, Richard D. E. Saunders², Paul F. Scott¹, Timothy W. Shimwell¹, David J. Titterton¹, Elizabeth M. Waldram¹ & Jonathon T. L. Zwart³

¹ *Astrophysics Group, Cavendish Laboratory, J J Thomson Avenue, Cambridge CB3 0HE*

² *Kavli Institute for Cosmology Cambridge, Madingley Road, Cambridge, CB3 0HA*

³ *Columbia Astrophysics Laboratory, Columbia University, 550 West 120th Street, New York 10027, USA*

Accepted —; received —; in original form 28 February 2019

ABSTRACT

We present $25''$ resolution radio images of five Lynds Dark Nebulae (L675, L944, L1103, L1111 & L1246) at 16 GHz made with the Arcminute Microkelvin Imager (AMI) Large Array. These objects were previously observed with the AMI Small Array to have an excess of emission at microwave frequencies relative to lower frequency radio data. In L675 we find a flat spectrum compact radio counterpart to the $850\,\mu\text{m}$ emission seen with SCUBA and suggest that it is cm-wave emission from a previously unknown deeply embedded young protostar. In the case of L1246 the cm-wave emission is spatially correlated with $8\,\mu\text{m}$ emission seen with *Spitzer*. Since the MIR emission is present only in *Spitzer* band 4 we suggest that it arises from a population of PAH molecules, which also give rise to the cm-wave emission through spinning dust emission.

Key words: Radiation mechanisms:general – ISM:general – ISM:clouds – stars:formation

1 INTRODUCTION

The complete characterization of microwave emission from spinning dust grains is a key question in both astrophysics and cosmology. It probes a region of the electromagnetic spectrum where a number of different astrophysical disciplines overlap. It is important for CMB observations in order to correctly characterise the contaminating foreground emission; for star and planetary formation it is important because it potentially probes a regime of grain sizes that is not otherwise easily observable.

Although a number of objects have now been found to exhibit anomalous microwave emission, attributed to spinning dust, it is still unclear what differentiates those objects from the many other

seemingly similar targets that do not show the excess. In the specific case of dark clouds the recent AMI sample (AMI Consortium: Scaife et al. 2009; hereinafter Paper I) of fourteen Lynds Dark Nebulae found an excess in only five.

It has been suggested that cm-wave emission from spinning dust is emitted by a population of ultra-small grains (Draine & Lazarian 1998). These ultra-small grains are thought to exist mainly in the form of single polycyclic aromatic hydrocarbon (PAH) molecules. PAH molecules are generally detected through their narrow line emission features in the MIR. For these emission features to be observed the PAH molecules must be exposed to a strong source of UV flux. Since this flux is generally absent in the case of dark clouds, the microwave emission from the rotation of PAH molecules may be the only way to study the very small grain population in these objects.

It is also known that radio continuum emission in dark clouds may arise from ionized gas associated with a stellar outflow. When

^{*} We request that any reference to this paper cites “AMI Consortium: Scaife et al. 2009”

† E-mail: as595@mrao.cam.ac.uk

a luminous star is present this arises either as the result of a compact HII region or an ionized stellar wind. In the case of very young low luminosity stars radio continuum emission may be also be detected. In this instance it is generally attributed to the presence of a partially ionized ($0.02 \leq x_e \leq 0.35\%$; Bacciotti & Eisloffel 1999) stellar wind (Wright & Barlow 1975; Panagia & Felli 1975), or possibly a neutral wind which has been shock-ionized further from the central source by impacting on a dense obstacle (Curiel et al. 1989).

In this paper we present follow-up observations of the five AMI Small Array (SA) spinning dust detections (Paper I) at higher resolution with the AMI Large Array (LA) over the same frequency range.

2 OBSERVATIONS

AMI comprises two synthesis arrays, one of ten 3.7 m antennas (SA) and one of eight 13 m antennas (LA), both sited at Lord’s Bridge, Cambridge (AMI Consortium: Zwart et al. 2008). The telescope observes in the band 13.5–17.9 GHz with cryostatically cooled NRAO indium–phosphide front-end amplifiers. The overall system temperature is approximately 25 K. Amplification, equalization, path compensation and automatic gain control are then applied to the IF signal. The backend has an analogue lag correlator with 16 correlations formed for each baseline at path delays spaced by 26 mm. In addition both real and imaginary correlations are formed by use of 0° and 180° hybrids. From these, eight 0.75 GHz bandwidth channels are synthesized. In practice, the two lowest frequency channels (1 & 2) are not generally used due to a lower response in this frequency range and interference from geostationary satellites.

Observations of five Lynds dark nebulae selected from the original AMI SA sample were made in 2009 February–March using the AMI LA. The co-ordinates of these fields are listed in Table 1 along with the size of the AMI LA synthesized beam towards each object and the r.m.s. noise measured outside the primary beam on the CLEANed maps. We note that the AMI LA observation of L1246 is towards the north-east of this cloud where anomalous emission was detected by the AMI SA and does not cover the same area as the original SCUBA observation.

Data reduction was performed using the local software tool REDUCE. This applies both automatic and manual flags for interference, shadowing and hardware errors, performs phase and amplitude calibrations and then Fourier transforms the correlator data to synthesize frequency channels before output to disk in *uv* FITS format suitable for imaging in AIPS. Flux calibration was performed using short observations of 3C286 near the beginning and end of each run. We assumed I+Q flux densities for this source in the AMI LA channels consistent with the frequency dependent model of Baars et al. (1977), ≈ 3.3 Jy at 16 GHz. As Baars et al. measure I and AMI LA measures I+Q, these flux densities include corrections for the polarisation of the calibrator source derived by interpolating from VLA 5, 8 and 22 GHz observations. A correction is also made for the changing intervening air mass over the observation. From other measurements, we find the flux calibration is accurate to better than 5 per cent (AMI Consortium: Scaife et al. 2008; AMI Consortium: Hurley–Walker et al. 2009). The phase was calibrated using interleaved observations of calibrators selected from the Jodrell Bank VLA Survey (JVAS; Patnaik et al. 1992). After calibration, the phase is generally stable to 5° for channels 4–7, and 10°

Table 1. AMI LA Lynds Dark Nebulae. Column [1] Name of cloud, [2] Right Ascension, [3] Declination, [4] AMI LA synthesized beam FWHM major axis, [5] AMI LA synthesized beam FWHM minor axis, and [6] r.m.s. noise fluctuations on the combined channel map.

Name	RA (J2000)	Dec (J2000)	$\Delta\theta_{\text{maj}}$ (arcsec)	$\Delta\theta_{\text{min}}$ (arcsec)	σ_{rms} ($\frac{\mu\text{Jy}}{\text{bm}}$)
L675	19 23 52.6	11 07 39	49.9	27.4	35
L944	21 17 40.8	43 18 08	36.5	31.2	31
L1103	21 42 10.2	56 43 44	32.0	26.3	25
L1111	21 40 27.1	57 48 10	39.4	30.8	29
L1246	23 25 30.1	63 38 30	31.2	26.9	25

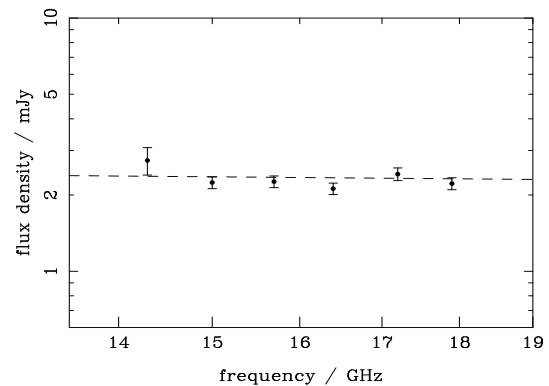


Figure 2. L675 Source A: data points are flux densities from AMI LA channels 3–8. The best-fit spectral index of $\alpha = 0.10 \pm 0.36$ is shown as a dashed line.

for channels 3 and 8. The FWHM of the primary beam of the AMI LA is $\approx 6'$ at 16 GHz.

Reduced data were imaged using the AIPS data package. CLEAN deconvolution was performed using the task IMAGR which applies a differential primary beam correction to the individual frequency channels to produce the combined frequency image. CLEAN deconvolution maps were made from both the combined channel set and for individual channels. The full set of CLEANed AMI maps is shown in Figure 1. The broad spectral coverage of AMI allows a representation of the spectrum between 14.3 and 17.9 GHz to be made independently of other telescopes and in what follows we use the convention: $S \propto \nu^{-\alpha}$, where S is flux density, ν is frequency and α is the spectral index. All errors are quoted to 1σ .

3 RESULTS

L675: The AMI LA observations of L675 show two obvious regions of compact emission, see Fig. 1. The first of these, slightly offset from the pointing centre, is coincident with both the peak of the AMI SA emission and also the compact emission seen at $850\mu\text{m}$ by the SCUBA instrument (Visser et al. 2001; 2002). We denote this source “A”. The second, just outside the LA primary beam FWHM to the north-east, is coincident with the probable extragalactic point source identified as “B” in the original AMI SA observations (Paper I).

Source A shows a flat spectrum across the AMI band, $\alpha_{14.3}^{17.9} = 0.10 \pm 0.36$, consistent with free-free emission, see Fig. 2.

L944: The original AMI SA observations of L944 revealed a compact region of emission to the north of the cloud, coinci-

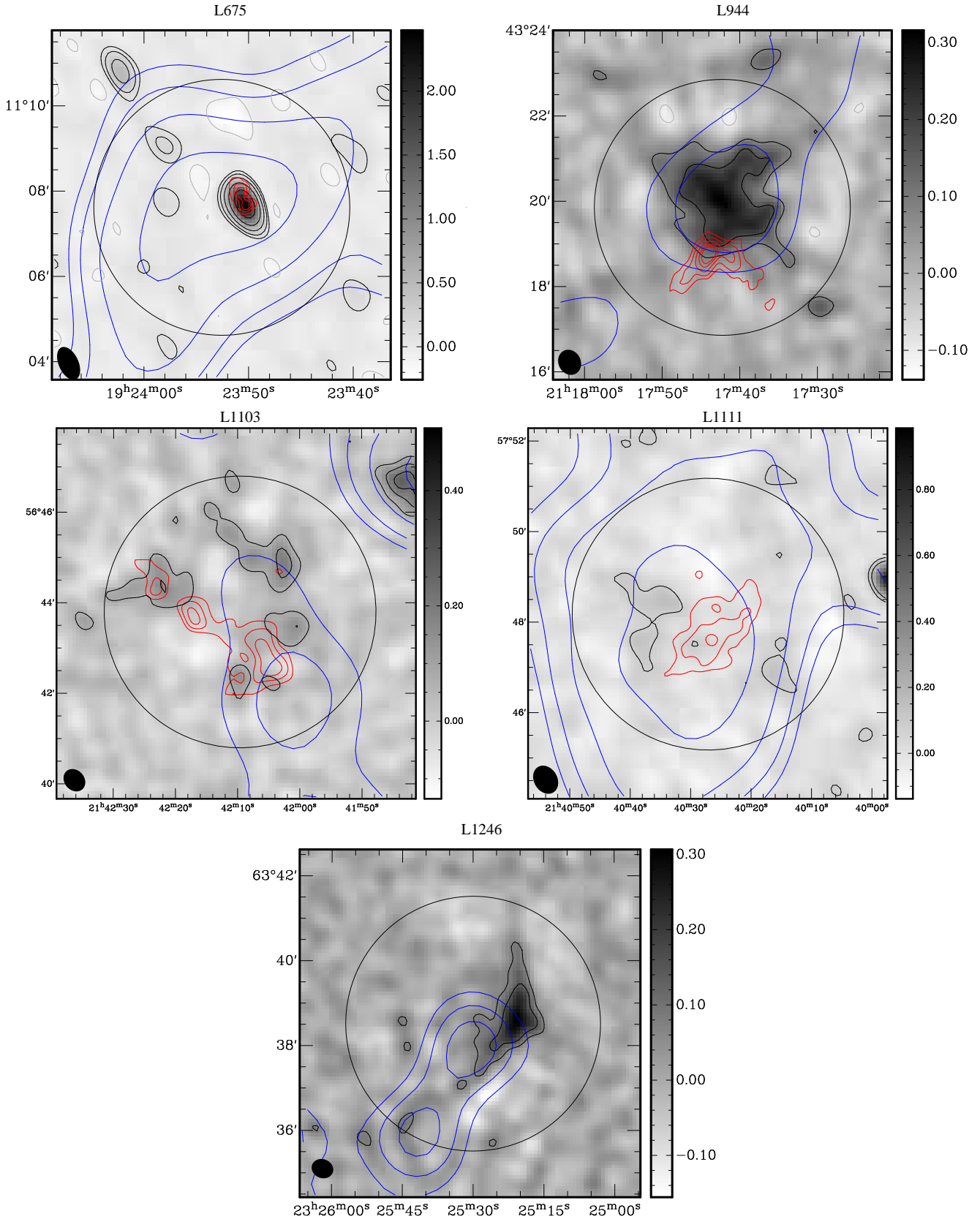


Figure 1. AMI LA combined channel data is shown as greyscale in units of mJy/beam and black contours at 3, 6, 12, 24 σ etc. SCUBA 850 μm data is shown as red contours with levels as in Visser et al. (2001;2002) for the clouds L675–L1111. The AMI LA observation of L1246 does not cover the region observed by SCUBA. AMI SA data is shown as blue contours with levels as in Paper I. The AMI LA primary beam FWHM is shown as a circle and the synthesized beam as a filled ellipse in the bottom left corner.

Table 2. Integrated flux densities in mJy for AMI LA observations of L675, L944 and L1246. Errors are calculated as $\sigma = \sqrt{(0.05S)^2 + \sigma_{\text{rms}}^2}$, where σ_{rms} is the r.m.s. noise in the individual channel map.

Name	Freq. (GHz)												α
	14.3		15.0		15.7		16.4		17.2		17.9		
L675	2.74	± 0.34	2.24	± 0.12	2.26	± 0.12	2.12	± 0.11	2.42	± 0.14	2.22	± 0.12	0.10 ± 0.36
L944	-		2.03	± 0.11	2.40	± 0.13	2.89	± 0.15	2.86	± 0.15	-		-2.11 ± 0.49
L1246	-		0.62	± 0.18	0.55	± 0.03	0.62	± 0.03	0.58	± 0.04	-		-0.40 ± 0.82

dent with one side of the protostellar outflow. AMI LA observations, see Fig. 1, reveal this emission arises not from a point-like object but rather from a diffuse region of emission. We estimate the flux spectrum by integrating the flux density from the primary beam corrected channel maps within a two arcminute radius of the LA pointing centre. This shows a steeply rising spectrum with $\alpha_{14.3}^{17.9} = -2.1 \pm 0.5$, which is consistent with that found from the AMI SA data. The large error on this index comes from the limited frequency coverage. The flux density found towards this region in the LA map is only marginally lower than that found from the comparatively much coarser resolution SA map. This implies that the emission comes not from one smooth extended region that is partially resolved out by the LA baselines, but from a collection of smaller fragments. These fragments are unresolved by either array, although the granularity becomes more evident in the higher frequency channels of the LA. The amount of flux lost in channels 5 to 8 relative to channel 4 is significantly smaller than would be expected from a Gaussian source of similar dimensions.

L1103 & L1111: AMI LA observations of L1103 and L1111 do not show any distinct regions of compact cm-wave emission. The diffuse patches of low level emission present within the primary beam towards both sources are indicative of larger scale structures which have been resolved out by the synthesized beam.

L1246: AMI SA observations towards L1246 did not show any excess emission coincident with the SCUBA identification of the dark cloud, but did reveal a region of emission $\approx 2'$ to the north-east of the cloud, in a region not covered by the SCUBA map, which had no counterpart in the lower frequency observations. AMI LA observations of this NE region show an arc of emission, see Fig. 1. We assess the spectral behaviour of this object in two ways. Firstly, we estimate the flux density of the arc itself. We fit and remove a tilted plane baselevel within an irregular polygon drawn around the object and integrate the remaining flux. Secondly, we fit a tilted plane baselevel to a circle at the primary beam FWHM and integrate all the flux above this baselevel within that radius. Both methods give consistent results, as might be expected since the primary beam is relatively empty otherwise. From the first method we find a spectral index $\alpha_{15.0}^{17.9} = -0.40 \pm 0.87$, and from the second $\alpha_{15.0}^{17.9} = -0.47 \pm 0.82$.

4 DISCUSSION

L675 and L1246 have archival *Spitzer* IRAC data, which shows in both cases a significant amount of emission in Band 4 (6.4–9.4 μm) and very little in the other three (3.2–3.9, 4.0–5.0 and 4.9–6.4 μm , respectively). In the case of L675 this emission is present on a very large scale, see Fig. 3. The emission seen at 16 GHz with the AMI SA appears on a similar scale, however the small field of view of the the *Spitzer* data precludes a more detailed comparison. Archival IRAS data towards this region provides no constraint on the low

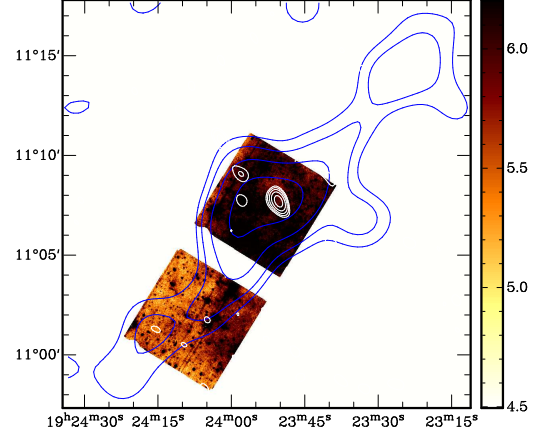


Figure 3. L675: AMI LA combined channel data is shown as white contours at 3, 6, 12 σ etc. *Spitzer* Band 4 data is shown as greyscale in MJy/sr, and is saturated at both ends to emphasise the structure present. AMI SA data is shown as blue contours as in Fig. 1.

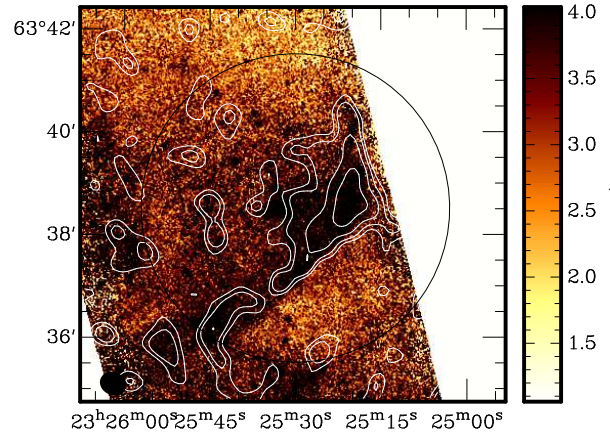


Figure 4. L1246: AMI LA combined channel data is shown as white contours at 1, 2, 4, 8 σ etc. *Spitzer* Band 4 data is shown as greyscale in MJy/sr, saturated at both ends of the scale to emphasise the structure present. The AMI LA primary beam is shown as a circle and the synthesized beam as a filled ellipse in the bottom left corner.

frequency side of the thermal dust greybody spectrum. Without further sub-mm data it is not possible to rule out the possibility that the emission seen by the AMI LA is consistent with the low frequency tail of the thermal dust emission. However, L1246 shows an arc of emission at 16 GHz which is also evident in *Spitzer* IRAC Band 4, see Fig. 4. This emission is again not present in Bands 1–3. In Band 4 it is present as an arc, coincident with that seen at 16 GHz in the AMI LA data.

Spitzer Band 4 contains two of the PAH emission lines, including the strongest ($7.7\ \mu\text{m}$). Of the three other *Spitzer* bands only Band 1 contains a PAH emission line ($3.3\ \mu\text{m}$), however this weak emission line is on the very edge of the bandpass and is likely to be heavily attenuated. It is probable therefore that the MIR correlated cm-wave data seen in the AMI maps is a consequence of spinning dust emission from a population of PAH molecules.

In the case of L675A, we must consider the possibility that we are observing a coincidental extragalactic radio source. Using the extended 9C survey 15 GHz source counts (Waldram et al. 2009), where $n(S) = 51(S/\text{Jy})^{-2.15} \text{Jy}^{-1} \text{sr}^{-1}$, the probability that a source with flux density greater than 2 mJy lies within the FWHM of the AMI LA primary beam is 0.12, and only 0.01 within the SCUBA field. It is likely therefore that the radio source L675A is associated with the SCUBA core.

The presence of a neutral or partially ionized wind from an outflow source that has been shocked through encountering a dense obstacle (Torrelles et al. 1985; Rodríguez et al. 1986) is used to understand the spectral indices seen towards exciting sources in the radio regime (Curiel et al. 1990; Cabrit & Bertout 1992). This model allows a spectral index range of -0.1 (optically thin) to 2 (optically thick), which explains results which deviate from the value of $\alpha = 0.6$ required by a spherically symmetric ionized wind (Wright & Barlow 1975; Panagia & Felli 1975). Using this model as described in Curiel et al. (1989;1990) the radio emission is expected to be optically thin ($\tau = 0.1$), consistent with the spectral index seen across the AMI band. Assuming a stellar wind with a wind speed of 200 km s^{-1} , we can calculate that the AMI flux densities towards L675A are consistent with a mass loss of $3.5 \times 10^{-7} M_{\odot} \text{ yr}^{-1}$. A mass loss such as this implies a mechanical luminosity from the wind of $L_{\text{mech}} \approx 1.1 L_{\odot}$, comparable to the values found by Curiel et al for L1448.

The nature of the emission seen towards L944 with the AMI LA is uncertain. The spectral index of this emission is consistent with spinning dust emission or alternatively the optically thick component of free-free spectrum. Such a free-free spectrum might be exhibited at 16 GHz by ultra-compact HII regions. However a turn-over frequency above 16 GHz would have an extremely high mass and should therefore be obvious in sub-mm observations.

5 CONCLUSIONS

We have used the AMI LA to observe a sample of five Lynds Dark Nebulae selected as candidates for spinning dust emission from the AMI SA sample of Lynds Dark Nebulae (Paper I). Towards two of these clouds (L1103 & L1111) we detect only patchy diffuse emission characteristic of the presence of a larger structure which has been mostly resolved out.

Towards L675 we have observed flat spectrum compact cm-wave emission coincident with the SCUBA $850\ \mu\text{m}$ emission from the same region. These characteristics suggest that this source is associated with a stellar wind from a deeply embedded young protostar, which has been shocked at a distance of $\approx 10 \text{ AU}$.

We detect extended cm-wave emission to the North of the L944 SMM-1 protostar which displays spectral behaviour consistent with either spinning dust, or alternatively a collection of ultra-compact HII regions. This needs to be confirmed by either higher radio frequency measurements in order to measure the optically thin region of the spectrum and the turn-over, or sub-mm measurements to place constraints on the mass of such a region. Such a

high turn-over frequency would require a high emission measure and correspondingly high mass.

L1246 shows an arc of cm-wave emission which is coincident with emission seen in *Spitzer* Band 4. We suggest that this is an example of emission from a population of PAH molecules, seen in emission lines in the *Spitzer* data, and emission as a consequence of rapid rotation of the molecules in the cm-wave data.

6 ACKNOWLEDGEMENTS

We thank the staff of the Lord's Bridge Observatory for their invaluable assistance in the commissioning and operation of the Arcminute Microkelvin Imager. The AMI is supported by Cambridge University and the STFC. NHW, CRG, TS, TF, MO and MLD acknowledge the support of PPARC/STFC studentships. This work is based in part on archival data obtained with the Spitzer Space Telescope, which is operated by the Jet Propulsion Laboratory, California Institute of Technology under a contract with NASA. Support for this work was provided by an award issued by JPL/Caltech.

REFERENCES

- AMI Consortium: Hurley-Walker N., et al., 2009, MNRAS, 396, 365
- AMI Consortium: Scaife A. M. M., et al., 2009, arXiv, arXiv:0908.1655
- AMI Consortium: Scaife A. M. M., et al., 2008, MNRAS, 385, 809
- AMI Consortium: Zwart J. T. L., et al., 2008, MNRAS, 391, 1545
- Baars J. W. M., Genzel R., Pauliny-Toth I. I. K., Witzel A., 1977, A&A, 61, 99
- Bacciotti F., Eisloffel J., 1999, A&A, 342, 717
- Cabrit S., Bertout C., 1992, A&A, 261, 274
- Clemens D. P., Yun J. L., Heyer M. H., 1991, ApJS, 75, 877
- Curiel S., Raymond J. C., Moran J. M., Rodriguez L. F., Canto J., 1990, ApJ, 365, L85
- Curiel S., Rodriguez L. F., Bohigas J., Roth M., Canto J., Torrelles J. M., 1989, ApL&C, 27, 299
- Draine B. T., Lazarian A., 1998, ApJ, 508, 157
- Lada C. J., 1985, ARA&A, 23, 267
- Panagia N., Felli M., 1975, A&A, 39, 1
- Patnaik A. R., Browne I. W. A., Wilkinson P. N., Wrobel J. M., 1992, MNRAS, 254, 655
- Torrelles J. M., Ho P. T. P., Rodriguez L. F., Canto J., 1985, ApJ, 288, 595
- Rodriguez L. F., Canto J., Torrelles J. M., Ho P. T. P., 1986, ApJ, 301, L25
- Visser A. E., Richer J. S., Chandler C. J., 2001, MNRAS, 323, 257
- Visser A. E., Richer J. S., Chandler C. J., 2002, AJ, 124, 2756
- Waldram E. M., Pooley G. G., Davies M. L., Grainge K. J. B., Scott P. F., 2009, arXiv, arXiv:0908.0066
- Wright A. E., Barlow M. J., 1975, MNRAS, 170, 41

This paper has been typeset from a \LaTeX file prepared by the author.